

LIBSVX: A Supervoxel Library and Benchmark for Early Video Processing

Chenliang Xu · Jason J. Corso

Received: date / Accepted: date

Abstract Supervoxel segmentation has strong potential to be incorporated into early video analysis as superpixel segmentation has in image analysis. However, there are many plausible supervoxel methods and little understanding as to when and where each is most appropriate. Indeed, we are not aware of a single comparative study on supervoxel segmentation. To that end, we study seven supervoxel algorithms, including both off-line and streaming methods, in the context of what we consider to be a good supervoxel: namely, spatiotemporal uniformity, object/region boundary detection, region compression and parsimony. For the evaluation we propose a comprehensive suite of seven quality metrics to measure these desirable supervoxel characteristics. In addition, we evaluate the methods in a supervoxel classification task as a proxy for subsequent high-level uses of the supervoxels in video analysis. We use six existing benchmark video datasets with a variety of content-types and dense human annotations. Our findings have led us to conclusive evidence that the hierarchical graph-based (GBH), segmentation by weighted aggregation (SWA) and temporal superpixels (TSP) methods are the top-performers among the seven methods. They all perform well in terms of segmentation accuracy, but vary in regard to the other desiderata: GBH captures object boundaries best; SWA has the best potential for region compression; and TSP achieves the best undersegmentation error.

Keywords supervoxels · segmentation and grouping · video segmentation · spatiotemporal processing

C. Xu (✉) · J. J. Corso
Electrical Engineering and Computer Science
University of Michigan,
1301 Beal Avenue
Ann Arbor, MI 48109-2122, USA
E-mail: cliangxu@umich.edu

J. J. Corso
E-mail: jjcorso@eecs.umich.edu

1 Introduction

Images have many pixels; videos have more. It has thus become standard practice to first preprocess images and videos into more tractable sets by either extraction of salient points (Schmid and Mohr, 1997) or oversegmentation into superpixels (Ren and Malik, 2003). Preprocessing output—salient points or superpixels—is more perceptually meaningful than raw pixels, which are merely a consequence of digital sampling (Ren and Malik, 2003). However, the same practice does not entirely exist in video analysis. Although many methods do indeed initially extract salient points or dense trajectories, e.g., Laptev (2005), we are aware of few methods that rely on a supervoxel segmentation, which is the video analog to a superpixel segmentation. In fact, those papers that do preprocess video tend to rely on a per-frame superpixel segmentation, e.g., Lee et al (2011), or use a full-video segmentation, e.g., Grundmann et al (2010).

The basic position of this paper is that supervoxels have great potential in advancing video analysis methods, as superpixels have for image analysis. To that end, we perform a thorough comparative evaluation of seven supervoxel methods: five off-line and two streaming methods. The off-line methods require the video to be available in advance and short enough to fit in memory. They load the whole video at once and process it afterwards. The five off-line methods we choose—segmentation by weighted aggregation (SWA) (Sharon et al, 2000, 2006; Corso et al, 2008), graph-based (GB) (Felzenszwalb and Huttenlocher, 2004), hierarchical graph-based (GBH) (Grundmann et al, 2010), mean shift (Paris and Durand, 2007), and Nyström normalized cuts (NCut) (Fowlkes et al, 2004; Shi and Malik, 2000; Fowlkes et al, 2001)—broadly sample the methodology-space, and are intentionally selected to best analyze methods with differing qualities for supervoxel segmentation. For example, both SWA and NCut use the normalized cut criterion as the underlying

ing objective function, but SWA minimizes it hierarchically whereas NCut does not. Similarly, there are two graph-based methods that optimize the same function, but one is subsequently hierarchical (GBH). We note that, of the off-line methods, only GBH had been proposed intrinsically as a supervoxel method; each other one is either sufficiently general to serve as one or has been adapted to serve as one. We also note a similar selection of segmentation methods has been used in the (2D) image boundary comparative study (Arbelaez et al, 2011) and nonetheless our selections share a good overlap with the ones studied in the recent video segmentation benchmark (Galasso et al, 2013).

In contrast, streaming methods require only constant memory (depends on the streaming window range) to execute the algorithm which makes them feasible for surveillance or to run over a long video on a less powerful machine. The two streaming methods we choose—streaming hierarchical video segmentation (streamGBH) (Xu et al, 2012) and temporal superpixels (TSP) (Chang et al, 2013) employ different strategies to treat video data. The streamGBH approximates a full video segmentation by both hierarchical and temporal Markov assumptions. Each time it segments video frames within a streaming window, and the length of the streaming window can be as short as one frame or as long as the full video, which equates it to full-video GBH segmentation. TSP represents a set of methods (Chang et al, 2013; Van den Bergh et al, 2013; Reso et al, 2013) that computes the superpixel segmentation on the first frame and then extends the superpixels to subsequent frames (one by one) in a video. The TSP method (Chang et al, 2013) uses a Gaussian Process for the streaming segmentation.

Our paper pits the five off-line and two streaming methods in an evaluation on a suite of metrics designed to assess the methods on basic supervoxel desiderata (Sect. 2.2), such as following object boundaries and spatiotemporal coherence. The specific metrics we use are 3D undersegmentation error, 3D segmentation accuracy, boundary recall distance and label consistency. They evaluate the supervoxel segmentations against human annotations. We also use a set of human-independent metrics: explained variation, mean size variation and temporal extent of supervoxels, which directly explore the properties of each method. Finally, we compare the supervoxel methods in a particular application—supervoxel classification—that evaluates methods in a recognition task, which we consider to be a proxy to various high-level video analysis tasks in which supervoxels could be used. We use six complementary video datasets to facilitate the study: BuffaloXiph (Chen and Corso, 2010), SegTrack v2 (Tsai et al, 2010; Li et al, 2013), CamVid (Brostow et al, 2008), BVDS (Sundberg et al, 2011; Galasso et al, 2013), Liu et al (2008a) and Middlebury Flow (Baker et al, 2011). They span from few videos to one hundred videos, and from sparse annotations to dense frame-by-frame annotations.

A preliminary version of our work appears in Xu and Corso (2012). Since its initial release, the LIBSVX benchmark has been widely used in supervoxel method evaluation by the community, including but not limited to Xu et al (2012, 2013); Chang et al (2013); Palou and Salembier (2013); Reso et al (2013); Van den Bergh et al (2013); Lee and Choi (2014); de Souza et al (2014); Tripathi et al (2014). In this paper, we complement the library with the two streaming methods and a set of new benchmark metrics on new video datasets. In addition, we add a new experiment of supervoxel classification to evaluate methods in terms of a middle-level video representation towards high-level video analysis. We also note that a recent video segmentation evaluation is proposed in Galasso et al (2013). We distinguish our work from them by evaluating directly on supervoxel segmentation, the oversegmentation of a video, and using various datasets including densely labeled human annotations with a set of novel benchmark metrics. It is our position that evaluations of both over-segmentation and segmentation in video are necessary to establish a thorough understanding of the problem-space within the computer vision community.

Our evaluation yields conclusive evidence that GBH, SWA and TSP are the top-performers among the seven methods. They all perform well in terms of segmentation accuracy, but vary in regard to the other desiderata: GBH captures object boundaries best; SWA has the best potential for region compression; and TSP follows object parts and achieves the best undersegmentation error. Although GBH and SWA, the two offline methods, are quite distinct in formulation and may perform differently under other assumptions, we find a common feature among the two methods (and one that separates them from the others) is the manner in which coarse level features are incorporated into the hierarchical computation. TSP is the only streaming method among the three and generates supervoxels with the best spatiotemporal uniformity. Finally, the supervoxel classification experiment further supports our findings and shows a strong correlation to our benchmark evaluation.

The complete supervoxel library, benchmarking code, classification code and documentation are available for download at <http://www.supervoxels.com>. Various supervoxel results on major datasets in the community (including the existing six datasets Chen and Corso (2010); Tsai et al (2010); Li et al (2013); Brostow et al (2008); Sundberg et al (2011); Galasso et al (2013); Liu et al (2008a); Baker et al (2011)) are also available at this location to allow for easy adoption of the supervoxel results by the community.

The rest of the paper is organized as follows. We present a theoretical background in Sect. 2 and a brief description of the methods in Sect. 3. We introduce the datasets and processing setup in Sect. 4. We thoroughly discuss comparative performance in terms of benchmark in Sect. 5 and super-

voxel classification in Sect. 6. Finally, we conclude the paper in Sect. 7.

2 Background

2.1 Superpixels

The term *superpixel* was coined by Ren and Malik (2003) in their work on learning a binary classifier that can segment natural images. The main rationale behind superpixel over-segmentation is twofold: (1) pixels are not natural elements but merely a consequence of the discrete sampling of the digital images and (2) the number of pixels is very high making optimization over sophisticated models intractable. Ren and Malik (2003) use the normalized cut algorithm (Shi and Malik, 2000) for extracting the superpixels, with contour and texture cues incorporated. Subsequently, many superpixel methods have been proposed (Levinshtein et al (2009); Veksler et al (2010); Moore et al (2008); Liu et al (2011); Zeng et al (2011) or adopted as such (Felzenszwalb and Huttenlocher, 2004; Vincent and Soille, 1991; Comaniciu and Meer, 2002) and used for a variety of applications: e.g., human pose estimation (Mori et al, 2004), semantic pixel labeling (He et al, 2006; Tighe and Lazebnik, 2010), 3D reconstruction from a single image (Hoiem et al, 2005) and multiple-hypothesis video segmentation (Vazquez-Reina et al, 2010) to name a few. Few superpixel methods have been developed to perform well on video frames, such as Drucker and MacCormick (2009) who base the method on minimum cost paths but do not incorporate any temporal information.

2.2 What makes a good supervoxel method?

First, we define a *supervoxel*—the video analog to a superpixel. Concretely, given a 3D lattice Λ^3 (the voxels in the video), a supervoxel v is a subset of the lattice $v \subset \Lambda^3$ such that the union of all supervoxels comprises the lattice and they are pairwise disjoint: $\bigcup_i v_i = \Lambda^3 \wedge v_i \cap v_j = \emptyset \forall i, j$ pairs. Obviously, various image/video features may be computed on the supervoxels, such as color histograms and textons. In this initial definition, there is no mention of certain desiderata that one may expect, such as locality, coherence, and compactness. Rather than include them in mathematical terms, we next list terms of this sort as desirable characteristics of a *good* supervoxel method.

We define a good supervoxel method based jointly on criteria for good supervoxels, which follow closely from the criteria for good segments (Ren and Malik, 2003), and the actual cost of generating them (videos have an order of magnitude more pixels over which to compute). Later, in our experimental evaluation, we propose a suite of benchmark metrics designed to evaluate these criteria (Section 5).

Spatiotemporal Uniformity. The basic property of spatiotemporal uniformity, or *conservatism* (Moore et al, 2008), encourages compact and uniformly shaped supervoxels in space-time (Levinshtein et al, 2009). This property embodies many of the basic Gestalt principles—proximity, continuation, closure, and symmetry—and helps simplify computation in later stages (Ren and Malik, 2003). Furthermore, Veksler et al (2010) show that for the case of superpixels, compact segments perform better than those varying in size on the higher level task of salient object segmentation. For temporal uniformity (called coherence in Grundmann et al (2010)), we expect a mid-range compactness to be most appropriate for supervoxels (bigger than, say, five frames and less than the whole video).

Spatiotemporal Boundaries and Preservation. The supervoxel boundaries should align with object/region boundaries when they are present and the supervoxel boundaries should be stable when they are not present; i.e., the set of supervoxel boundaries is a superset of object/region boundaries. Similarly, every supervoxel should overlap with only one object (Liu et al, 2011). Furthermore, the supervoxel boundaries should encourage a high-degree of *explained variation* (Moore et al, 2008) in the resulting oversegmentation. If we consider the oversegmentation by supervoxels as a compression method in which each supervoxel region is represented by the mean color, we expect the distance between the compressed and original video to have been minimized.

Computation. The computation cost of the supervoxel method should reduce the overall computation time required for the entire application in which the supervoxels are being used.

Performance. The oversegmentation into supervoxels should not reduce the achievable performance of the application. Our evaluation will not directly evaluate this characteristic (because we study the more basic ones above).

Parsimony. The above properties should be maintained with as few supervoxels as possible (Liu et al, 2011).

3 Methods

We study seven supervoxel methods—mean shift (Paris and Durand, 2007), graph-based (GB) (Felzenszwalb and Huttenlocher, 2004), hierarchical graph-based (GBH) (Grundmann et al, 2010), streaming hierarchical graph-based (stream-GBH) (Xu et al, 2012), Nyström normalized cut (NCut) (Shi and Malik, 2000; Fowlkes et al, 2001, 2004), segmentation by weighted aggregation (SWA) (Sharon et al, 2000, 2006; Corso et al, 2008) and temporal superpixels (Chang et al, 2013)—that broadly sample the methodology-space among statistical and graph partitioning methods (Arbelaez et al, 2011). We have selected these seven due to their respective traits and their inter-relationships: for example, Nyström and

SWA both optimize the same normalized cut criterion, and streamGBH extends GBH to handle arbitrarily long videos and still keeps the hierarchy property.

We describe the methods in some more detail below. We note that *many* other methods have been proposed in the computer vision literature for video segmentation, e.g., Vincent and Soille (1991); Greenspan et al (2004); Brendel and Todorovic (2009); Liu et al (2008b); Vazquez-Reina et al (2010); Veksler et al (2010); Khan and Shah (2001); Megret and DeMenthon (2002); Budvytis et al (2011); Galasso et al (2012), but we do not cover them in any detail in this study. We also do not cover strictly temporal segmentation, e.g. Patel and Sethi (1997).

3.1 Mean Shift

Mean shift is a mode-seeking method, first proposed by Fukunaga and Hostetler (1975). Comaniciu and Meer (2002) and Wang et al (2004) adapt the kernel to the local structure of the feature points, which is more computationally expensive but improves segmentation results. Original hierarchical mean shift in video (DeMenthon and Megret, 2002; Paris, 2008) improves the efficiency of (isotropic) mean-shift methods by using a streaming approach. The mean shift algorithm used in our paper is presented by Paris and Durand (2007), who introduce Morse theory to interpret mean shift as a topological decomposition of the feature space into density modes. A hierarchical segmentation is created by using topological persistence. Their algorithm is more efficient than previous works especially on videos and large images. We use the author-provided implementation¹ to generate a supervoxel hierarchy and then stratify the pairwise merging into a fixed-level of hierarchy.

3.2 Graph-Based (GB)

Felzenszwalb and Huttenlocher (2004) propose a graph-based algorithm for image segmentation; it is arguably the most popular superpixel segmentation method. Their algorithm runs in time nearly linear in the number of image pixels, which makes it suitable for extension to spatiotemporal segmentation. Initially, each pixel, as a node, is placed in its own region R , connected with 8 neighbors. Edge weights measure the dissimilarity between nodes (e.g. color differences). They define the internal difference of a region, $Int(R)$, as the largest edge weight in the minimum spanning tree of R . Traversing the edges in a non-decreasing weight order, the regions R_i and R_j incident to the edge are merged if the current edge weight is less than the relaxed minimum

internal difference of the two regions:

$$\min(Int(R_i) + \tau(R_i), Int(R_j) + \tau(R_j)) , \quad (1)$$

where $\tau(R) = k/|R|$ is used to trigger the algorithm and gradually makes it converge. k is a scale parameter that reflects the preferred region size. The algorithm also has an option to enforce a minimum region size by iteratively merging low-cost edges until all regions contain the minimum size of pixels. We have adapted the algorithm for video segmentation by building a 3D lattice over the spatiotemporal volume, in which voxels are nodes connected with 26 neighbors in the lattice (9 to the previous and the next frames, 8 to the current frame). One challenge in using this algorithm is the selection of an appropriate k for a given video, which the hierarchical extension (GBH, next) overcomes. We use a set of k as well as various minimum region sizes to generate the segmentation output for our experiment.

3.3 Hierarchical Graph-Based (GBH)

The hierarchical graph-based video segmentation algorithm is proposed by Grundmann et al (2010). Their algorithm builds on an oversegmentation of the above spatiotemporal graph-based segmentation. It then iteratively constructs a region graph over the obtained segmentation, and forms a bottom-up hierarchical tree structure of the region (segmentation) graphs. Regions are described by local Lab histograms. At each step of the hierarchy, the edge weights are set to be the χ^2 distance between the Lab histograms of the connected two regions. They apply the same technique as above, Felzenszwalb and Huttenlocher (2004), to merge regions. Each time they scale the minimum region size as well as k by a constant factor s . Their algorithm not only preserves the important region borders generated by the oversegmentation, but also allows a selection of the desired segmentation hierarchy level h , which is much better than directly manipulating k to control region size. We set a large h to output segmentations with various numbers of supervoxels.

3.4 Graph-Based Streaming Hierarchical (streamGBH)

Graph-based streaming hierarchical video segmentation is proposed in our earlier work (Xu et al, 2012) to extend GBH (Grundmann et al, 2010) to handle arbitrarily long videos in a streaming fashion and still maintain the segmentation hierarchy. The algorithm approximates the full video GBH segmentations by both a hierarchical and a temporal Markov assumption, allowing a small number of frames to be loaded into a memory at any given time. Therefore the algorithm runs in a streaming fashion. In our comparison experiments, we set a fixed streaming window size (10 frames) for all

¹ <http://people.csail.mit.edu/sparis/>

subsequences and, again, a large h as in GBH to output segmentations with various numbers of supervoxels.

3.5 Nyström Normalized Cut (NCut)

Nyström Normalized Cuts (Shi and Malik, 2000) as a graph partitioning criterion has been widely used in image segmentation. A multiple eigenvector version of normalized cuts is presented in Fowlkes et al (2004). Given a pairwise affinity matrix W , they compute the eigenvectors V and eigenvalues Γ of the system

$$(D^{-1/2}WD^{-1/2})V = V\Gamma, \quad (2)$$

where D is a diagonal matrix with entries $D_{ii} = \sum_j W_{ij}$. Each voxel is embedded in a low-dimensional Euclidean space according to the largest several eigenvectors. The k-means algorithm is then be used to do the final partitioning. To make it feasible to apply to the spatiotemporal video volume, Fowlkes et al (2001) use the Nyström approximation to solve the above eigenproblem. Their paper demonstrates segmentation on relatively low-resolution, short videos (e.g., $120 \times 120 \times 5$) and randomly samples points from the first, middle, and last frames.

However, in our experiments, NCut is not scalable as the number of supervoxels and the length of video increases. Sampling too many points makes the Nyström method require too much memory, while sampling too few gives unstable and low performance. Meanwhile, the k-means clustering algorithm is sufficient for a video segmentation with few clusters, but a more efficient clustering method is expected regarding the number of supervoxels. Therefore, we run NCut for a subset of our experiments with lower solution and we set 200 sample points. We run k-means on 20% of the total voxels and k-nearest neighbor search to assign supervoxel labels for all voxels.

3.6 Segmentation by Weighted Aggregation (SWA)

SWA is an alternative approach to optimizing the normalized cut criterion (Sharon et al, 2000, 2006; Corso et al, 2008) that computes a hierarchy of sequentially coarser segmentations. The method uses an algebraic multigrid solver to compute the hierarchy efficiently. It recursively coarsens the initial graph by selecting a subset of nodes such that each node on the fine level is *strongly coupled* to one on the coarse level. The algorithm is nearly linear in the number of input voxels, and produces a hierarchy of segmentations, which motivates its extension to a supervoxel method. The SWA implementation is based on our earlier 3D-SWA work in the medical imaging domain (Corso et al, 2008).

3.7 Temporal Superpixels (TSP)

The temporal superpixels method computes the superpixel segmentation on the first frame and then extends the existing superpixels to subsequent frames in a video. Therefore, this set of methods Chang et al (2013); Van den Bergh et al (2013); Reso et al (2013), by their nature, are computing supervoxels in a streaming fashion, which is similar to streamGBH with a streaming window of one frame. We choose Chang et al (2013) as the representative method for evaluation. The algorithm first extends the SLIC (Achanta et al, 2012) superpixel algorithm to form a generative model for constructing superpixels. Each pixel is modeled using five dimensional feature vector: three channel color and the 2D location in image. Superpixels are inferred by clustering with a mixture model on individual features as a Gaussian with known variance. After generating superpixels for the first frame, the algorithm applies a Gaussian Process with a bilateral kernel to model the motion between frames. We use the implementation² provided by the authors with the default parameters to run the algorithm in evaluation.

4 Datasets

We make use of six video datasets for our experimental purposes, with varying characteristics. The datasets have human-annotator drawn groundtruth labels at a frame-by-frame basis (four out of six) or at densely sampled frames in the video (two out of six). The sizes of the selected datasets vary from a few videos to one hundred videos. The set of datasets we choose are BuffaloXiph (Chen and Corso, 2010), SegTrack v2 (Li et al, 2013; Tsai et al, 2010), BVDS (Sundberg et al, 2011; Galasso et al, 2013), CamVid (Brostow et al, 2008), Liu et al (2008a) and Middlebury Flow (Baker et al, 2011). The datasets are originally built solving different video challenges: BuffaloXiph is gathered for pixel label propagation in videos; SegTrack is built for object tracking; BVDS has contributed to occlusion boundary detection; CamVid is taken in driving cars for road scene understanding; and Liu et al (2008a) and Middlebury Flow (Baker et al, 2011) are used for optical flow estimation. Rather than evaluating supervoxel methods on a single dataset, we conduct the evaluation on all six datasets (with only label consistency metric on Liu et al (2008a) and Middlebury Flow (Baker et al, 2011)), as the datasets are complementary and we believe supervoxels have potential to be a first processing step towards various video applications and problems. We briefly describe the six datasets used in our experiments.

BuffaloXiph from Chen and Corso (2010) is a subset of the well-known `xiph.org` videos that have been supple-

² <http://people.csail.mit.edu/jchang7/code.php>

mented with a 24-class semantic pixel labeling set (the same classes from the MSRC object segmentation dataset Shotton et al (2009)). The eight videos in this set are densely labeled with semantic pixels that leads to a total of 638 labeled frames, with a minimum of 69 frames-per-video (fpv) and a maximum of 86 fpv. The dataset is originally used for pixel label propagation (Chen and Corso, 2010) and videos in the dataset are stratified according to camera motion, object motion, the presence of articulated objects, the complexity of occlusion between objects and the difficulty of label propagation. Distinct regions with the same semantic class label are not separated in this dataset.

SegTrack v2 from Li et al (2013) is an updated version of the *SegTrack* dataset (Tsai et al, 2010) and provides frame-by-frame pixel-level foreground objects labeling rather than the semantic class labeling as in BuffaloXiph. It contains a total of 14 video sequences with 24 objects over 947 annotated frames. The videos in the dataset are stratified according to different segmentation challenges, such as motion blur, appearance change, complex deformation, occlusion, slow motion and interacting objects.

BVDS is initially introduced in Sundberg et al (2011) for occlusion boundary detection and then used for evaluating video segmentation algorithms by Galasso et al (2013). It consists of 100 HD quality videos with a maximum of 121 fpv and videos in the dataset are stratified according to occlusion, object categories and sizes, and different kinds of camera motion: translational, scaling and perspective motion. Each video is labeled with multiple human annotations by a sampling rate of 20 frames. We use all 100 videos in the evaluation ignoring the training/testing split (because BVDS is used only in the unsupervised parts of our evaluation).

Furthermore, the dataset has three different groupings for videos with moving objects, non-rigid motion, and considerable camera motion. Our experimental results show that all methods preserve the same performance order over these three video groupings, except TSP has better temporal extent than GB when only using videos with considerable camera motion. We show this additional result in the supplement.

CamVid from Brostow et al (2008) provides five long video sequences recorded at daytime and dusk from a car driving through Cambridge, England. The videos are composed by over ten minutes high quality 30Hz footage and are labeled with 11 semantic object class labels at 1Hz and in part 15Hz that leads to a total of 701 densely labeled frames. It also provides the training/test split, with two daytime and one dusk sequence for training and one daytime and one dusk sequence for testing. Therefore, this dataset in addition allows us to evaluate methods in terms of supervoxel semantic label

classification. We use all videos, in total 17898 frames³, in the evaluation in Sect. 5, and follow the training/test split in Sect. 6.

The remaining two datasets, **Liu et al (2008a)** and **Middlebury Flow** (Baker et al, 2011) are used for evaluating label consistency in Sect. 5.4. They are densely annotated with groundtruth flows. Liu et al (2008a) contains five videos with a minimum of 14 fpv and a maximum of 76 fpv. Middlebury Flow contains eight videos, but groundtruth for only two frames (one optical flow estimate) is available. We treat it as a special case where algorithms only process two frames.

4.1 Processing

To adapt all seven supervoxel methods to run through all videos in the datasets within reasonable time and memory consumption, we use BuffaloXiph, SegTrack v2 and Middlebury Flow at the original resolution; Liu et al (2008a) at half the original resolution; BVDS and CamVid, the two large datasets, at a quarter of the original HD resolution. One exception is NCut which runs at a fixed resolution of 240×160 on BuffaloXiph and SegTrack v2 datasets (the results are scaled up for comparison) and is not included in the experiments with BVDS and CamVid datasets due to its high computational demands. The comparison of NCut and other methods at the same downscaled resolution on BuffaloXiph and SegTrack are shown in our conference version of the paper (Xu and Corso, 2012), where the relative performance is similar to here.

We compare the seven methods as fairly as possible. However, each method has its own tunable parameters; we have tuned these parameters strictly to achieve a certain desired number of supervoxels per video (or per frame, depending on the experiment); parameters are tuned per method per dataset. For hierarchical methods, such as GBH, stream-GBH, SWA, a single run over a video can generate fine-to-coarse multiple levels of supervoxels. For Mean Shift, we tune the persistence threshold to get multiple stratified segmentations. For NCut, we vary the final step K-means clustering to get a set of supervoxels varying from 100 to 500 on BuffaloXiph and SegTrack v2. We use the suggested parameters by the authors for the two other methods (Mean Shift and TSP) and we provide all parameters to reproduce our experiments.

After we have generated a range of supervoxels for each video in a dataset, we use linear interpolation to estimate each methods' metric outputs for each video densely. The performance over a dataset at a certain number of supervoxels is drawn by averaging the interpolated values from all

³ We manually exclude the corrupted frames, and organize the dataset into short clips with roughly 100 frames-per-clip. The organized short clips can be downloaded from our website.

videos at the same number of supervoxels. This strategy can better align videos in a dataset and therefore avoids outliers with too many or too few supervoxels by simply taking averaged number of supervoxels over a dataset, especially when the videos are diverse in a dataset.

5 Benchmark Evaluation

Rather than evaluating the supervoxel methods on a particular application, as Hanbury (2008) does for superpixels and image segmentation, in this section we directly consider all of the base traits described in Sect. 2.2 at a fundamental level. We believe these basic evaluations have a great potential to improve our understanding of when a certain supervoxel method will perform well. Nonetheless, we further evaluate the performances of the supervoxel classification on the CamVid dataset in Sect. 6.

We note that some quantitative superpixel evaluation metrics have been recently used in Moore et al (2008); Levinstein et al (2009); Veksler et al (2010); Liu et al (2011); Zeng et al (2011). We select those most appropriate to validate our desiderata from Section 2.2. One way to conduct the experiments is by evaluating the frame-based measures and take the average over all the frames in the video. However, if we directly apply these methods to the supervoxel segmentation, the temporal coherence property can not be captured. Even a method without any temporal information can achieve a good performance in those 2D metrics, which have driven us to extend the above frame-based measures to the volumetric video-based measures when appropriate.

In the rest of this section, we first introduce a pair of volumetric video-based 3D metrics that score a supervoxel segmentation based on a given human annotation and they are 3D undersegmentation error (Sect. 5.1) and 3D segmentation accuracy (Sect. 5.2). We also evaluate the boundary recall distance of the supervoxel segmentation to the human drawn boundaries (Sect. 5.3), as well as measure the label consistency in terms of annotated groundtruth flows in a video (Sect. 5.4). Then we evaluate some basic properties of supervoxel segmentation that do not require human annotation, namely explained variation, mean size variation and temporal extent of supervoxels, in Sect. 5.5. We also report the computational cost of each supervoxel method (Sect. 5.6). We give visual comparison of the supervoxel segmentations against the groundtruth annotation in Fig. 6. Finally, we discuss our findings in Sect. 5.7.

5.1 3D Undersegmentation Error (UE3D)

Undersegmentation error in image segmentation was proposed in Levinstein et al (2009). It measures the fraction of pixels that exceed the boundary of the groundtruth segment

when overlapping the superpixels on it. We extend this concept to a spatiotemporal video volume to measure the space-time *leakage* of supervoxels when overlapping groundtruth segments. Given a video segmented into supervoxels $\mathbf{s} = \{s_1, s_2, \dots, s_n\}$ and a set of annotated groundtruth segments $\mathbf{g} = \{g_1, g_2, \dots, g_m\}$ in video, we define the following UE3D as the average fraction of the voxels that exceed the 3D volume of groundtruth segments:

$$\text{UE3D}(\mathbf{s}, \mathbf{g}) = \frac{1}{m} \sum_{i=1}^m \frac{\sum_{j=1}^n \text{Vol}(s_j | s_j \cap g_i \neq \emptyset) - \text{Vol}(g_i)}{\text{Vol}(g_i)}, \quad (3)$$

where $\text{Vol}(\cdot)$ denotes the amount of voxels that are contained in the 3D volume of a segment. Equation 3 takes the average score from all groundtruth segments \mathbf{g} . We note that the score from a single groundtruth segment g_i is not bounded. The metric imposes a greater penalty when supervoxels leak on smaller groundtruth segments. For example, if a video has a very small object, it will be equally weighted with a large object (e.g. background). Missing a pixel in the small object has a greater penalty than missing a background pixel. We also note that it is possible to set different weights for groundtruth segment classes when evaluating against a dataset with pixel semantic labels (e.g. BuffaloXiph). For a dataset with multiple human annotations (e.g. BVDS), we simply take the average score, which equally weights different human perceptions.

5.2 3D Segmentation Accuracy (SA3D)

Segmentation accuracy measures the average fraction of groundtruth segments that is correctly covered by the supervoxels: each supervoxel belongs to only one groundtruth segment (object) as a desired property from Sect. 2.2. We define the volumetric SA3D as

$$\text{SA3D}(\mathbf{s}, \mathbf{g}) = \frac{1}{m} \sum_{i=1}^m \frac{\sum_{j=1}^n \text{Vol}(s_j \cap g_i) \mathbb{1}[\text{Vol}(s_j \cap g_i) \geq \text{Vol}(s_j \cap \bar{g}_i)]}{\text{Vol}(g_i)}, \quad (4)$$

where $\bar{g}_i = \mathbf{g} \setminus \{g_i\}$ and the indicator function decides when there is an association of supervoxels between segment s_j and groundtruth segment g_i . Similar to UE3D, SA3D also takes the average score from all groundtruth segments \mathbf{g} . However, the score from a single groundtruth segment g_i is bounded in $[0, 1]$, where the extreme situations 1 and 0 are respectively define when g_i is perfectly partitioned by a set of supervoxels (e.g. Fig. 1(a)), and g_i is completely missed (e.g. Fig. 1(b)).

We note that UE3D and SA3D are complementary to evaluate an algorithm, as UE3D measures the leakage of

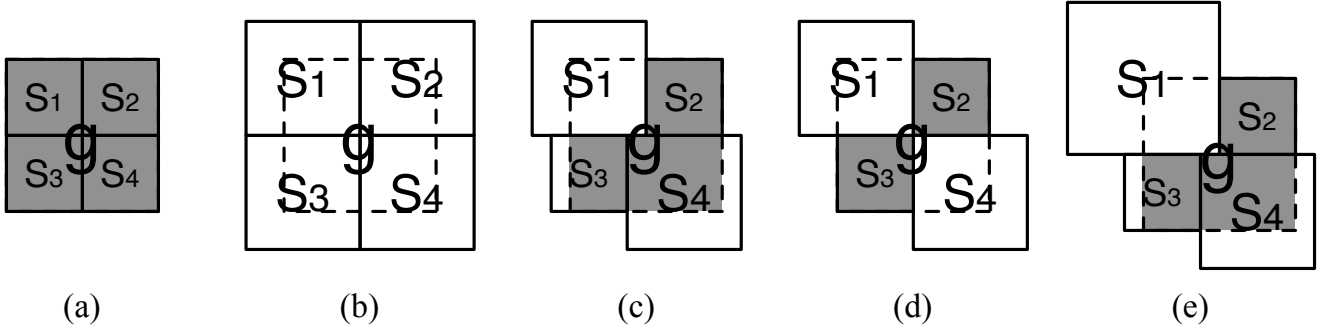


Fig. 1 A toy example of a single groundtruth segment g with five different supervoxel segmentations. We show the example in 2D for simple illustration. We draw the groundtruth segment g as a 2×2 dashed square shape. All supervoxel segments are shown in solid square shapes and are defined in three different sizes: 1×1 (e.g. s_1 in (a)), 1.5×1.5 (e.g. s_1 in (b)), and 2×2 (e.g. s_1 in (e)). Segment s_3 in (c) and (e) is offset by $1/4$. The gray areas are counted toward SA3D. The scores of UE3D, SA3D and BRD for each case are shown in Tab. 1.

all supervoxels touching a groundtruth segment and SA3D measures the fraction of the groundtruth segment that is correctly segmented. To further elucidate the differences between UE3D and SA3D, we show a toy example in Fig. 1 with scores shown in Tab. 1, where (c) and (d) have the same UE3D score but different SA3D scores, and (c) and (e) have the same SA3D score but different UE3D scores. (c) has the best scores for both UE3D and SA3D among all imperfect segmentation cases (b)-(e). Both the metrics are evaluated in space-time, such that they penalize supervoxels that break not only spatial boundaries but also temporal boundaries of the groundtruth segments—a good superpixel method can achieve high performance. However, it typically does so with a large number of supervoxels (the temporal extent is only one frame in this case) for the per-video basis. Therefore datasets with dense human annotations, such as BuffaloXiph and SegTrack v2, are more precise in terms of the 3D volumetric measures.

5.3 Boundary Recall Distance (BRD)

So far we have introduced a pair of 3D metrics defined by the set of groundtruth segments. They intrinsically use the groundtruth boundaries for locating the volume of the segments. We now directly evaluate the boundary recall distance, which measures how well the groundtruth boundaries are successfully retrieved by the supervoxel boundaries. We use BRD proposed in Chang et al (2013) to calculate the average distance from points on groundtruth boundaries to the nearest ones on supervoxel boundaries frame-by-frame in a video. It does not require a fixed amount of dilation for boundary matching as in typical boundary recall measures to offset small localization errors. The specific metric is defined as follows:

$$\text{BRD}(s, g) = \frac{1}{\sum_t |\mathcal{B}(g^t)|} \sum_{t=1}^T \sum_{i \in \mathcal{B}(g^t)} \min_{j \in \mathcal{B}(s^t)} d(i, j), \quad (5)$$

Metric	(a)	(b)	(c)	(d)	(e)
UE3D	0.00	1.25	0.63	0.63	1.06
SA3D	1.00	0.00	0.75	0.50	0.75
BRD	0.00	0.50	0.27	0.25	0.39

Table 1 The scores of UE3D, SA3D and BRD for the toy example in Fig. 1. The larger the better for SA3D, and the smaller the better for UE3D and BRD. The top two scores are bolded for each metric. BRD is calculated strictly for vertical boundary matching only and horizontal boundary matching only in this toy example, which is slightly different than Eq. 5.

where $\mathcal{B}(\cdot)$ returns the 2D boundaries of segments in a frame, $d(\cdot, \cdot)$ is the Euclidean distance between the two arguments, $|\cdot|$ denotes the amount of pixels contained by the argument at a frame, t indexes frames in a video (e.g. g^t denotes the set of all groundtruth segments on frame t), and i and j denote points on boundaries.

We also compute BRD for all cases in Fig. 1 and show the scores in Tab. 1. We note that BRD captures different aspects of an algorithm than UE3D and SA3D. For example, among the imperfect segmentation cases (b)-(e) (which are typical situations), (c) has the best scores in terms of UE3D and SA3D, but worse in BRD than (d) which is poor in SA3D. Therefore, there is no single segmentation that has the best scores for all three metrics (except the perfect partition in (a)) in this toy example.

5.4 Label Consistency (LC)

LC is also proposed in Chang et al (2013), which provides a possible way to measure how well supervoxels track the parts of objects given annotated groundtruth flows. Define $\mathcal{F} = \{F^{t-1 \rightarrow t} | t = 2, \dots, T\}$ as the vectorized groundtruth forward flow field in a video and $F^{t-1 \rightarrow t}(s_i)$ projects pixels contained in s_i at frame $t-1$ to pixels at frame t by the flow (subjected to the image boundary). The metric is defined as

follows:

$$\text{LC}(\mathbf{s}, \mathcal{F}) = \frac{\sum_{t=2}^T \sum_{i=1}^n |s_i^t \cap F^{t-1 \rightarrow t}(s_i)|}{\sum_{t=2}^T \sum_{i=1}^n |F^{t-1 \rightarrow t}(s_i)|}, \quad (6)$$

where s_i^t denotes the slice of supervoxel s_i at frame t , and the numerator measures the agreement of supervoxel labels and the projected labels by flow. We evaluate this metric on Liu et al (2008a) and Middlebury Flow where the ground-truth flow annotation is available.

5.5 Human-Independent Metrics

The following are human-independent metrics; in other words, they are not susceptible to variation in annotator perception that would result in differences in the human annotations, unlike the previous metrics. They directly reflect basic properties of the supervoxel methods, such as the temporal extent of generated supervoxels.

5.5.1 Explained Variation (EV)

The metric is proposed in Moore et al (2008) and it considers the supervoxels as a compression method of a video (Sect. 2.2):

$$\text{EV}(\mathbf{s}) = \frac{\sum_i (\mu_i - \mu)^2}{\sum_i (x_i - \mu)^2}, \quad (7)$$

where x_i is the color of the video voxel i , μ is the mean color of all voxels in a video and μ_i is the mean color of the supervoxel that contains voxel i . Erdem et al (2004) observe a correlation between EV and the human-dependent metrics for a specific object tracking task.

5.5.2 Mean Size Variation (MSV)

Chang et al (2013) propose superpixel size variation that measures the size variation of all superpixels in a video (as a set of frames). Here, we extend their metric to measure the size variation of the 2D slices of a supervoxel. MSV is the average score of such variation defined by all supervoxels in a video:

$$\text{MSV}(\mathbf{s}) = \frac{1}{n} \sum_{j=1}^n \sqrt{\frac{\sum_t \left((|s_i^t| - |\hat{s}_i|)^2 \mathbb{1}[|s_i^t| > 0] \right)}{\sum_t \mathbb{1}[|s_i^t| > 0] - 1}}, \quad (8)$$

where $|\hat{s}_i| = \frac{\sum_t |s_i^t|}{\sum_t \mathbb{1}[|s_i^t| > 0]}$ is the average size of 2D slices of a supervoxel. MSV favors the kind of supervoxels whose 2D sizes varies minimally over time.

	GB	GBH	streamGBH	SWA
Time (s)	115	1166	1000	934
Memory (GB)	6.9	9.4	1.6	19.9
	TSP	MeanShift	NCut	
Time (s)	1440	101	1198	
Memory (GB)	0.9	3.8	20.9	

Table 2 Computational cost.

5.5.3 Temporal Extent (TEX)

TEX measures the average temporal extent of all supervoxels in a video. The measure of supervoxel temporal extent is originally proposed in Xu et al (2012) as a way to compare different streaming video segmentation methods. Later, Chang et al (2013) extend the measure by normalizing over the number of frames contained in a video. We also use it here for the evaluation. The metric is defined as follows:

$$\text{TEX}(\mathbf{s}) = \frac{1}{nT} \sum_{i=1}^n \sum_{t=1}^T \mathbb{1}[|s_i^t| > 0]. \quad (9)$$

5.6 Computational Cost

We report the computational cost of all methods for a typical video with $352 \times 288 \times 85$ voxels—we record the time and peak memory consumption on a laptop featured with Intel Core i7-3740QM @ 2.70GHz and 32GB RAM running Linux, see Table 2. All methods are implemented in C except NCut (Matlab) and TSP (Matlab with MEX). Furthermore, all methods are single threaded except NCut running with 8 threads with resized resolution to 240×160 .

5.7 Discussion

We evaluate seven methods over six datasets by the metrics defined above. We focus the evaluation in the range of 0 to 2000 supervoxels per-video (Fig. 2 and Fig. 4) as well as 0 to 1500 supervoxels per-frame (Fig. 3 and Fig. 5). We do the best to accommodate all methods in the above range, but not all methods can generate the full range of plots (e.g. Mean Shift requires huge memory to generate over 500 supervoxels per-frame for a typical video). The visualization of supervoxel segmentations can be found in Fig. 6. For the rest of this section, we first discuss the choice of two plot bases in Sect. 5.7.1, then conclude our findings in Sect. 5.7.2.

5.7.1 Plot Bases

We plot the results with two types of plot bases, namely the number of supervoxels per-video and per-frame. We summarize the rationale below, which basically distinguishes the two bases according to how space and time are treated.

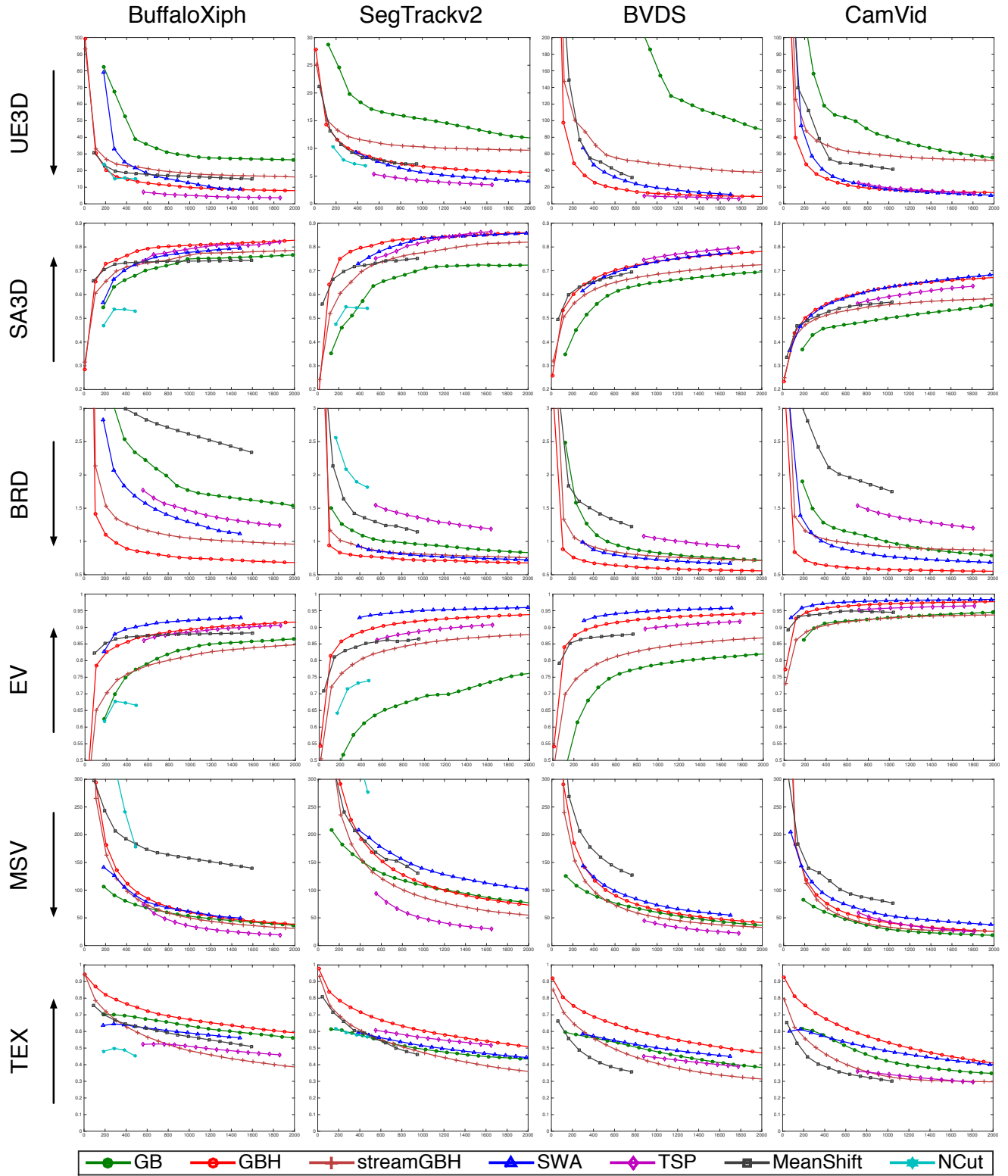


Fig. 2 Graphs plot the number of supervoxels **per-video** (x-axis) against various metrics (y-axis). Datasets are organized by columns and metrics are organized by rows. Black arrows in each row are used to indicate the direction of better performance with regard to the metric. Plot ranges along the y-axis are aligned for all metrics except UE3D. Plotted dots are the average score of linear-interpolated values from all videos in a dataset at the same number of supervoxels per-video.

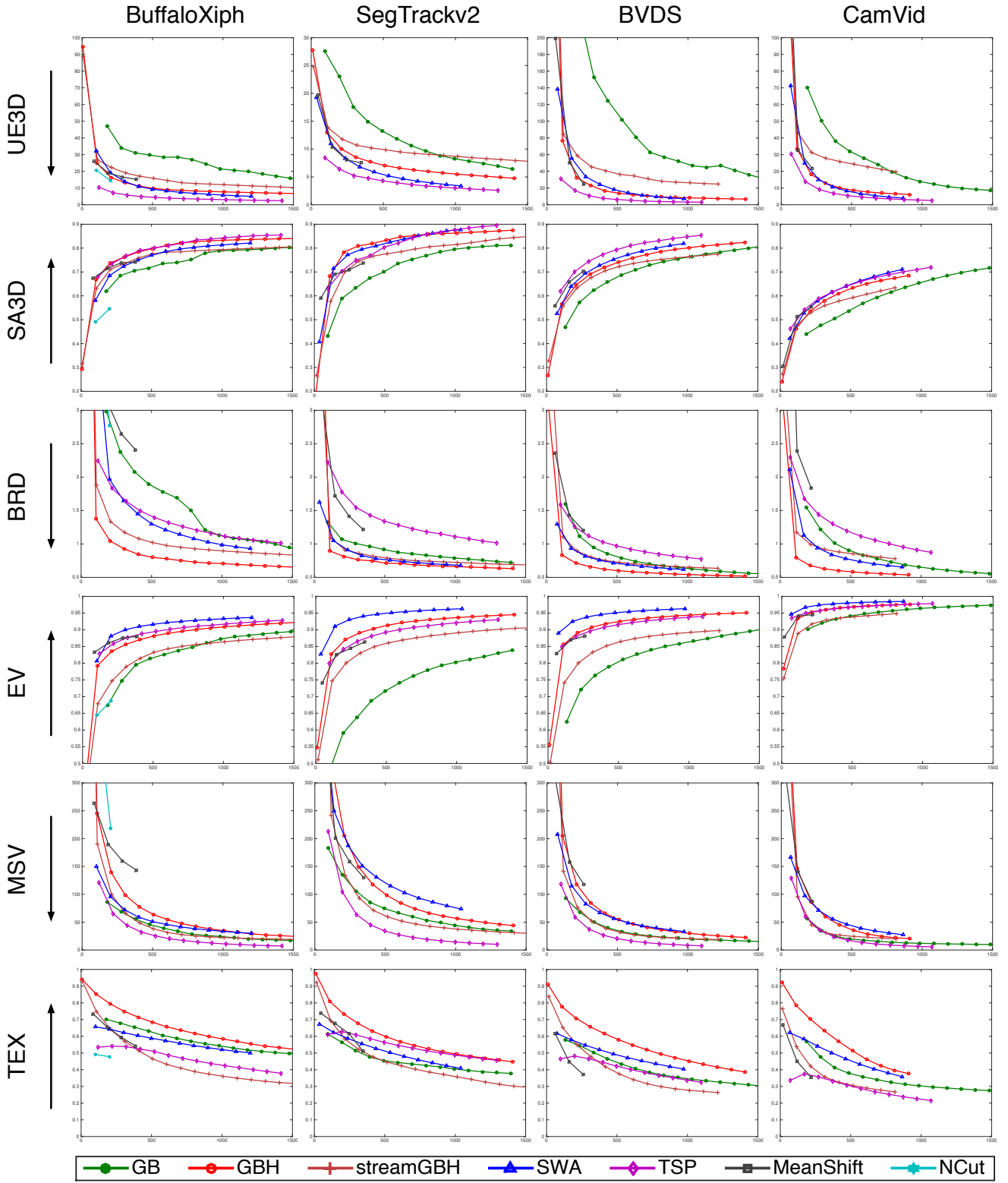


Fig. 3 Graphs plot the number of supervoxels **per-frame** (x-axis) against various metrics (y-axis). Datasets are organized by columns and metrics are organized by rows. Black arrows in each row are used to indicate the direction of better performance with regard to the metric. Plot ranges along the y-axis are aligned for all metrics except UE3D. Plotted dots are the average score of linear-interpolated values from all videos in a dataset at the same number of supervoxels per-frame.

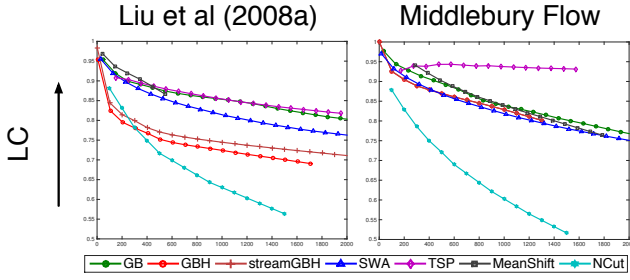


Fig. 4 Plots for Label Consistency (LC) against the number of supervoxels **per-video** (x-axis). Black arrow indicates the direction of better performance. Plotted dots are the average score of linear-interpolated values from all videos in a dataset at the same number of supervoxels per-video.

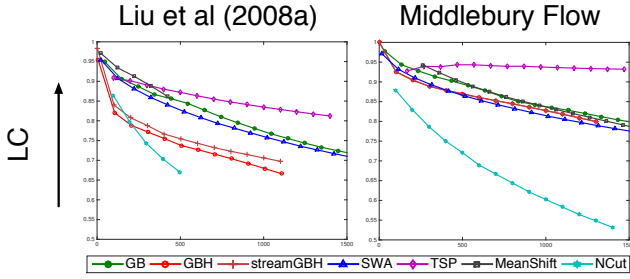


Fig. 5 Plots for Label Consistency (LC) based on the number of supervoxels **per-frame** (x-axis). Black arrow indicates the direction of better performance. Plotted dots are the average score of linear-interpolated values from all videos in a dataset at the same number of supervoxels per-frame.

Number of Supervoxels Per-Video (spv). In the earlier version of our paper (Xu and Corso, 2012), the number of supervoxels per-video is used for plotting figures of metric scores. Here, time is considered as an analogous, third dimension and treated accordingly, as in the definition of supervoxels. Hence, for example, one can consider this as a means of evaluating the compression-rate of a video as a whole. However, it may incorrectly relate videos of different lengths.

Number of Supervoxels Per-Frame (spf). Chang et al (2013) use the number of supervoxels per-frame (in this case, it is the same as the number of superpixels per-frame) in their evaluation. The mindset behind that differentiates the time dimension in a video from the spatial dimensions, such that the plot basis is not subject to different video lengths or motion. However, this approach fails to account for the temporal qualities of supervoxels—a good superpixel method can do well. For example, UE3D degenerates to UE2D for a superpixel method because it has perfect temporal boundaries.

Summary. We hence present plots against both bases and we discuss their comparisons.

5.7.2 Top Performing Methods

The metrics using human annotations, namely UE3D, SA3D, BRD and LC, reflect different preferences for supervoxels (see Sect. 2.2). A perfect segmentation can have all the best scores with respect to these metrics, while, often, a typical segmentation has its strengths in a subset of the metrics (recall the example in Fig. 1). Therefore, we organize our findings of the top performing methods by each metric and discuss the differences among datasets, if any. Recall that our choices of datasets in Sect. 4 represent many different types of video data (e.g. SegTrack v2 has only foreground object labels, and BuffaloXiph has pixel-level semantic class labels). Below we list the key results.

UE3D. For most cases, TSP has the best performance followed by SWA and GBH. The three methods have nearly the same good performance on CamVid for spv in Fig. 2. However, TSP stands out when evaluating for spf in Fig. 3.

SA3D. GBH performs best on BuffaloXiph for spv, whereas TSP performs best when plotted by spf. GBH, SWA and TSP perform almost equally well on SegTrack v2. TSP performs best on BVDS, where annotators are instructed to label all objects on sampled frames of a video. SWA and GBH perform equally best on CamVid for spv, but when plotting by spf, SWA and TSP perform the best.

BRD. GBH is the clear winner method in this metric, and following that are streamGBH and SWA. GB has a faster trend to approach GBH than streamGBH on CamVid and BVDS for spf.

LC. TSP (the only method uses optical flow in the implementations we use) has the best performance and there is a clear performance gap on Middlebury Flow, where videos only have two frames (Fig 4 and 5). Furthermore, unlike the other methods, the performance of TSP does not dramatically decrease when spv and spf increase on Middlebury Flow.

EV. SWA has the overall best performance and followed by GBH and TSP. GBH ranks better than TSP on BuffaloXiph for spv, but the ordering swapped when plotting against spf.

MSV. TSP has the best performance followed by streamGBH and GB except on CamVid for spv, where GB performs the best.

TEX. GBH has the longest temporal extent for both spv and spf within the range we plotted. We note Chang et al (2013) show that TSP has better performance than GBH in a different spectrum of spf on Liu et al (2008a) and SegTrack (Tsai et al, 2010).

Over all seven methods, GB and Mean Shift are the most efficient in time. Interestingly, neither GB nor Mean Shift performs best in any of the human annotation related quality measures—there is an obvious trade-off between the computational cost of the methods and the quality of their output (in terms of our metrics).

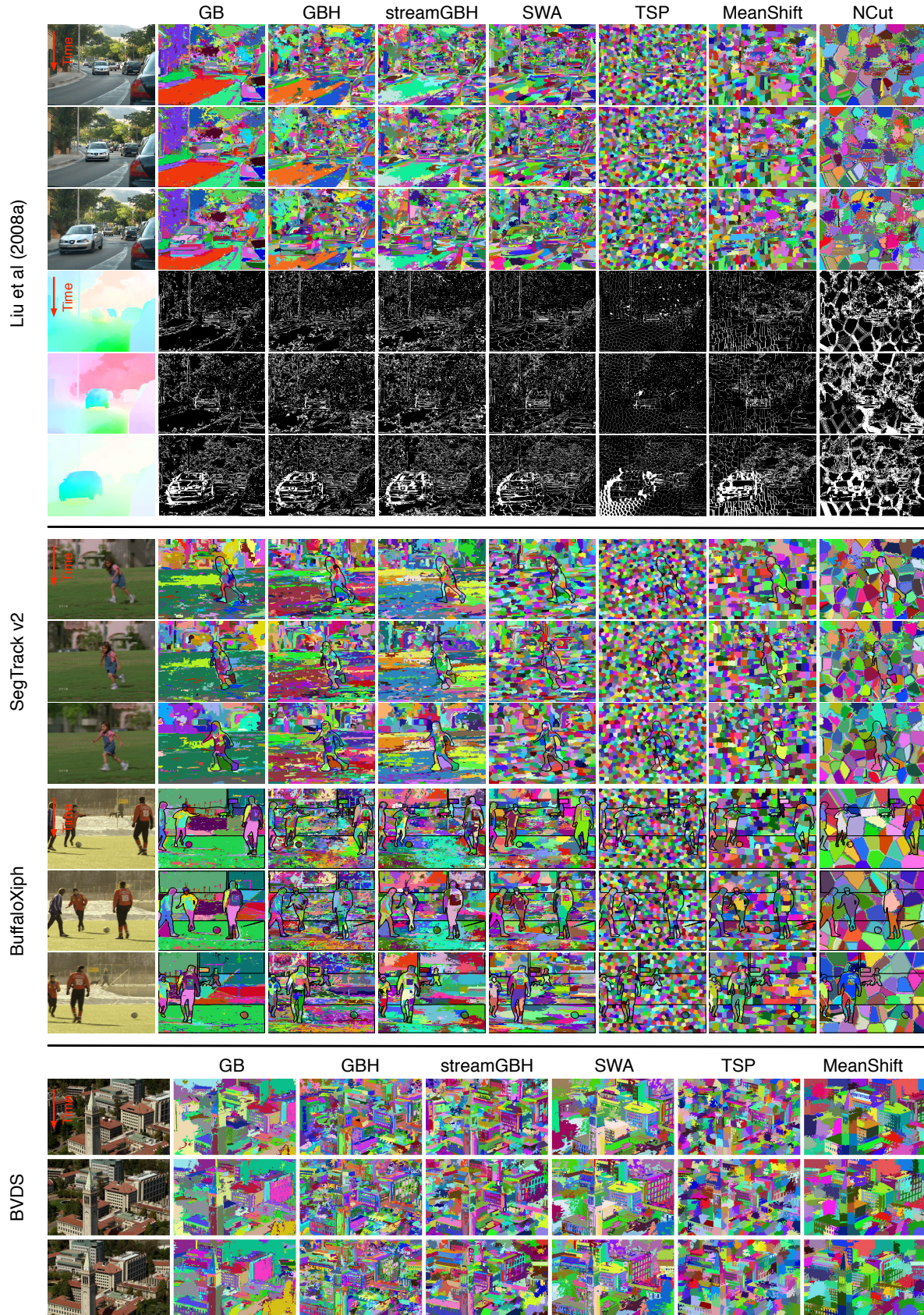


Fig. 6 Visual comparative results of the seven methods on videos. Each supervoxel is rendered with its distinct color and these are maintained over time. We recommend viewing these images zoomed on an electronic display. In the top part, we show a video from Liu et al (2008a) where label consistency is computed and shown in black and white (white pixels indicate inconsistency with respect to groundtruth flow). In the middle part, we show videos from SegTrack v2 and BuffaloXiph, where groundtruth object boundaries are drawn in black lines. We show a video from BVDS on the bottom.

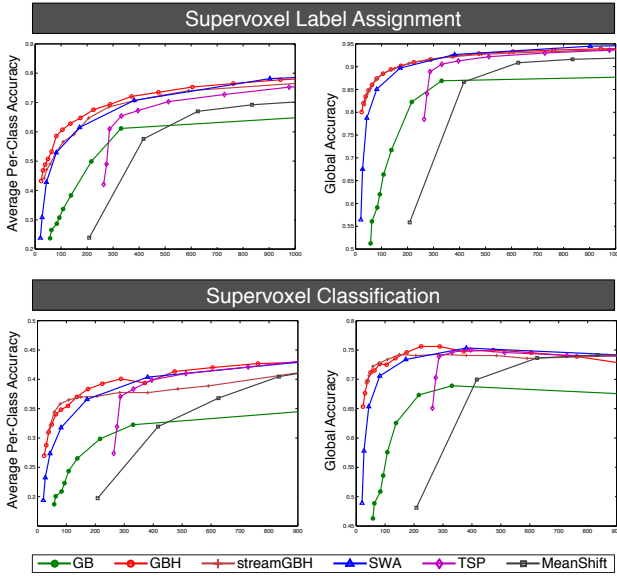


Fig. 7 Plots on the top are the pixel-level average per-class accuracy (left) and global accuracy (right) for both training and testing sets when supervoxels directly take groundtruth labels (the most frequent ones in volumes). Plots on the bottom are the pixel-level classification performance on the test set with SVMs trained on supervoxels. We show the plots in the range of 100 to 900 supervoxels every 100 frames (x-axis). The plotted dots are from actual segmentations rather than interpolated values. We note that Brostow et al (2008) report 53.0% average per-class and 69.1% global accuracy using random forests trained on pixels with both appearance and geometric cues, where we only use appearance cues with supervoxels.

We have focused on the facts here. Although understanding *why* these various algorithms demonstrate this comparative performance is an ultimate goal of our work, it is beyond the scope of this paper and would require a substantially deeper understanding of how space and time relate in video analysis. To overcome this limitation, we map these comparative performances onto specific problem-oriented needs in the Conclusion (Sect. 7).

6 Supervoxel Classification

In this section, we evaluate the supervoxel methods in a particular application: supervoxel semantic label classification. We use this application as a proxy to various high-level video analysis problems. For example, superpixel classification scores are frequently used as the unary term when building subsequent graphical model for scene understanding in images, e.g., Gould et al (2009). We use the CamVid dataset for this task due to its widely use in semantic pixel labeling in videos. Recall that CamVid has videos over ten minutes and labeled frames with 11 semantic classes at 1Hz, such as building, tree, car and road. We follow the standard training/test split: two daytime and one dusk sequence for training, and one daytime and one dusk sequence for testing.

We process the videos into supervoxel segmentations as described in Sect. 4.1. We use all supervoxel methods except for the NCut method because of its high memory requirement for these CamVid data, which rendered the size of the supervoxels too large to train meaningful classifiers.

Supervoxel Features. Tighe and Lazebnik (2010) extract a set of low-level features on superpixels and use the supervoxels generated by Grundmann et al (2010) for their video parsing on CamVid dataset. We apply a similar set of features with some modifications to suit for our task. We first dilate the 2D slices of supervoxels by 3 pixels and then extract features histograms from supervoxel volumes. To be specific, we compute histogram of textons⁴ and dense SIFT descriptors with 100 dimensions each. We also compute two types of color histograms, RGB and HSV, with 8 bins each channel. We describe the location of a supervoxel volume by averaging the distances of bounding boxes of its 2D slices to image boundaries. In addition to image features, we calculate dense optical flow and quantize flows in a supervoxel volume to 8 bins each according to vertical and horizontal velocity, and speed magnitude. Note that the way we extract the feature histograms is different than Tighe and Lazebnik (2010), where they use one representative superpixel of a supervoxel (the 2D slice with largest region). We think that the volume has better potential to represent the change of a supervoxel over time. We also note that more sophisticated video features can be added to supervoxel volumes such as dense trajectories (Wang et al, 2013) and HOG3D (Kläser et al, 2008). However, for a fair comparison of supervoxel methods, we stick to the dense image features and optical flow in order to prevent favoring one supervoxel method than another.

Supervoxel Labels. We assign a supervoxel with the most frequent groundtruth label occur in its volume and ignore supervoxels that fail to touch groundtruth frames (labeled at 1Hz on CamVid). We note that this step is distinct from most image superpixel classification work, e.g., Gould et al (2009), since videos are often sparsely labeled while images are densely labeled. Therefore, this step may introduce more noise in both training and testing than the image superpixel classification work, and it is closely related to two of our benchmark metrics—UE3D in Sect. 5.1 and SA3D in Sect. 5.2. We apply the pixel-level average per-class accuracy and global pixel accuracy to evaluate this *supervoxel label assignment* step and the top part in Fig. 7 shows the performance for all six methods in the experiment. Rather than using linear interpolated values as in Fig. 2 to 5, the plotted dots here map to actual segmentations generated by a single run of the algorithm over the dataset, and the plot basis is the number of supervoxels for every 100 frames.

⁴ <http://www.robots.ox.ac.uk/~vgg/research/textclass/filters.html>

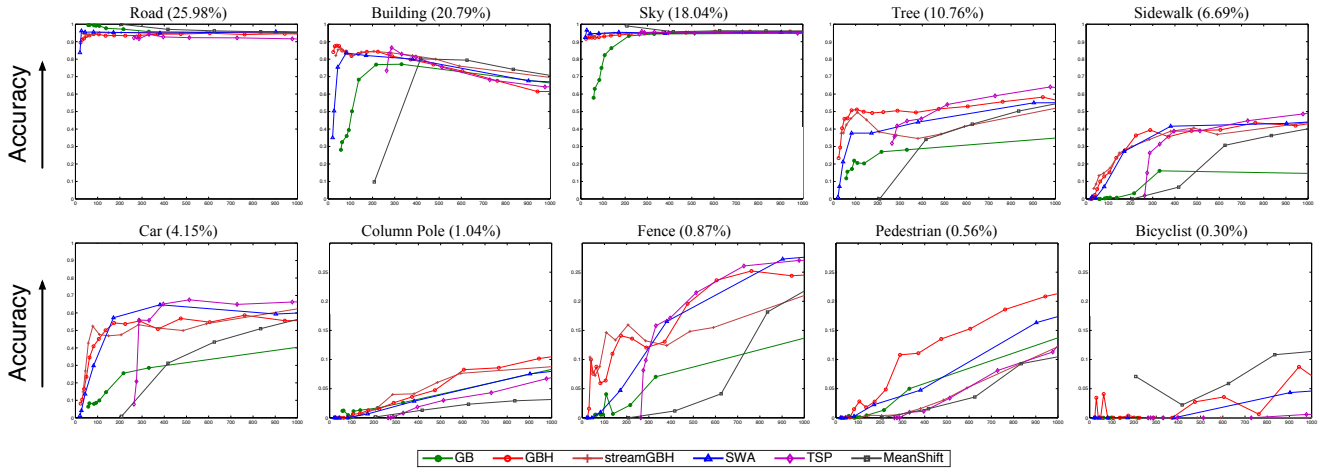


Fig. 8 Pixel-level labeling accuracy for each semantic class in the CamVid dataset, where the percentages of total pixels for each class are shown on top. All plots are shown in the range of 0 to 1000 supervoxels every 100 frames (x-axis). The first six plots (horizontal) are plotted with an accuracy range from 0 to 1, and the other plots are from 0 to 0.3. We do not show the class *Sign Symbol* (0.17%) here due to its low accuracy for all methods.

Classification Performance. Finally, we use linear SVMs⁵ on supervoxels to get the classification results on the test set. The output segmentations are for the entire video but we evaluate only on the labeled frames. We again show the performance in terms of pixel-level average per-class and global accuracy in the bottom part in Fig. 7 with the number of supervoxels ranging from less than 100 to more than 900 every 100 frames. To compare with pixel-based image segmentation method, we note that Brostow et al (2008) report 53.0% average per-class and 69.1% global accuracy by using both appearance and geometric cues. The supervoxel-based methods with our setup in general achieve a better global pixel performance but a worse average per-class accuracy (e.g. 500 supervoxels in Fig. 7) with respect to the range of supervoxel numbers we sampled for the evaluation. We suspect that some classes with small regions, such as *sign symbol* and *bicyclist*, become too small to capture when we scale the videos down to a much lower resolution (a quarter of the original) to accommodate all six supervoxel methods.

Fig. 8 shows the pixel-level labeling accuracy for each class in the dataset. For large classes, such as *road* and *sky*, all methods perform almost equally well regardless of the change of supervoxel numbers, except the performance for *building*, which rises then falls. This rise and fall results in a decrease in the overall global performance (see bottom right in Fig. 7). We explain this rise and fall behavior of the building class due to the overall scale-varying texture of buildings and the challenge to learn classifiers on them that perform equally well at different scales; for example, smaller supervoxels will cover small portions of buildings, say windows or bricks, which have distinct visual charac-

teristics, yet a single classifier is to be learned (in our evaluation). For other classes the performance increases when adding more supervoxels, and different methods have distinct performance on different classes. For example, GBH leads the score on *pedestrian* while TSP and SWA are the methods of choice on *car*. Further investigation is needed to better understand these nuances.

Fig. 9 shows visual comparison of six methods on two clips from the daytime test video. Although GB and Mean Shift successfully segment the *sidewalk* in the supervoxel segmentation, they miss a large portion of the *sidewalk* in the labeling, while the other methods capture it well. The *tree* tends to be better labeled by GBH. All methods segment the moving cars well. However none of the method get the small *sign symbol* in the second clip. We also show the results during dusk in Fig. 10. GB works poorly here; the greedy algorithm of GB is highly sensitive to local color thus it easily produces large incorrect segments. TSP visually segments *bicyclist* well regardless the incorrect boundaries. We think this is due to the compact shape of supervoxels that TSP generated can better track the superpixels on the bicyclist and prevent easily merging with other large segments such as *sidewalk*, *tree* and *road*. However, it also brings more fragmented segments on large smooth regions, such as *road* and *sidewalk* and weak boundary accuracy.

Overall, GBH, SWA and TSP achieve equally strong performance in the supervoxel classification experiment (see Fig. 7), and, again, they are the top performing ones in terms of our benchmark evaluation in Sect. 5. Methods such as GB and MeanShift have poor classification performance also perform less well on the benchmark metrics. For the streaming methods, streamGBH achieves very similar performance to its full-video counterpart GBH.

⁵ <http://www.csie.ntu.edu.tw/~cjlin/libsvm/>

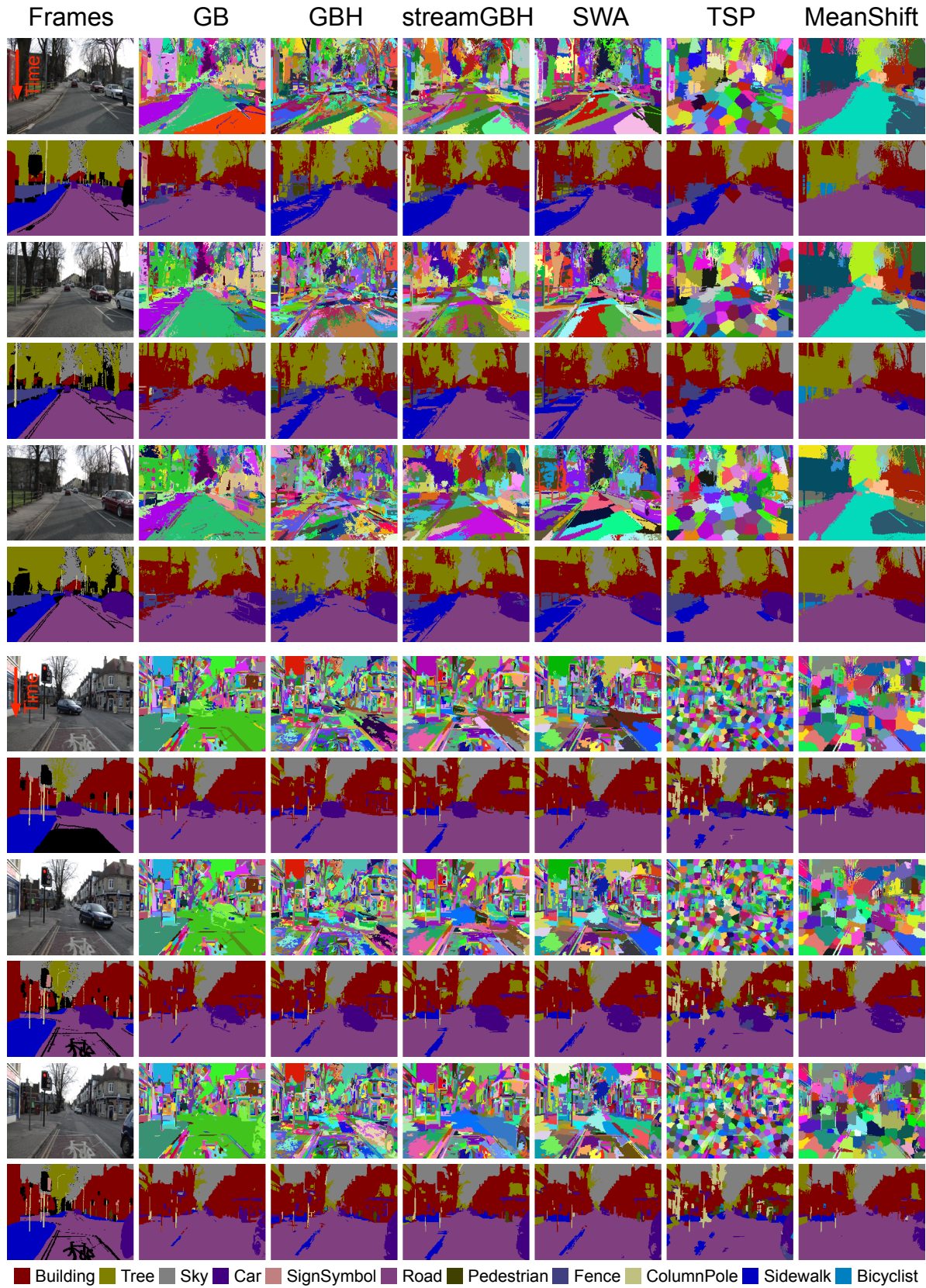


Fig. 9 Example results on two short clips from the CamVid daytime test video. Images in the first column are video frames and groundtruth labels and the remaining columns are individual methods with supervoxel segmentation and semantic labeling on supervoxels.

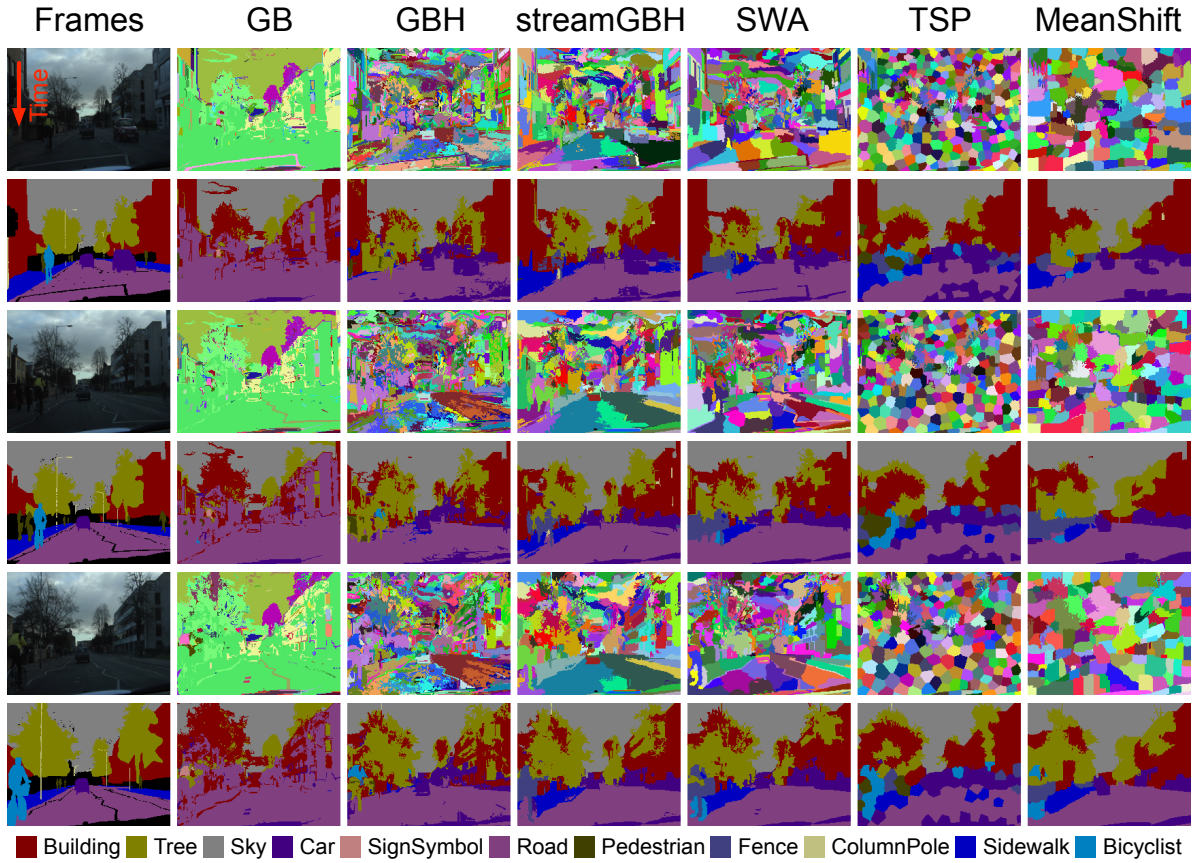


Fig. 10 Example results on a clip from the CamVid dusk test video. Images in the first column are video frames and groundtruth labels and the remaining columns are individual methods with supervoxel segmentation and semantic labeling on supervoxels.

7 Conclusion

We have presented a thorough evaluation of seven supervoxel methods including both off-line and streaming methods on a set of seven benchmark metrics designed to evaluate supervoxel desiderata as well as the recognition performance on a particular application. Samples from the datasets segmented under all seven methods are shown in Fig. 6, Fig. 9, and Fig. 10. These visual results convey the overall findings we have observed in the quantitative experiments. GBH, SWA and TSP are the top-performers among the seven methods in both our benchmark evaluation and the classification task. They all share a common feature in that they perform well in terms of segmentation accuracy, but they comparatively vary in performance in regard to the other metrics. GBH captures object boundaries best making it well suited for video analysis tasks when accurate boundaries are needed, such as robot manipulation. SWA has the best performance in the explained variation metric, which makes it most well-suited for compression applications. TSP follows object parts and achieves the best undersegmentation error making it well-suited for fine-grained activity analysis and other high-level video understanding problems. It seems ev-

ident that the main distinction behind the best offline methods, namely GBH and SWA, is the way in which they both compute the hierarchical segmentation. Although the details differ, the common feature among the two methods is that during the hierarchical computation, coarse-level aggregate features replace or modulate fine-level individual features. In contrast, TSP processes a video in a streaming fashion and also produces supervoxels that are the most compact and regular in shape. These differences suggest a complementarity that has the potential to be combined into a new method, which are currently investigating.

In this paper, we have explicitly studied the general supervoxel desiderata regarding a set of proposed benchmark metrics including both human annotation dependent and independent ones. In addition, we compare the supervoxel methods in a particular application—supervoxel classification that evaluates methods in a recognition task, which we consider to be a proxy to various high-level video analysis tasks in which supervoxels could be used. A strong correlation is presented between the benchmark evaluation and the recognition task. Methods, such as GBH, SWA and TSP, that achieve the top performance in the benchmark evaluation also perform best in the recognition task. The obvious question to

ask is how well will the findings translate to other application-specific ones, such as tracking and activity recognition. A related additional point that needs further exploration for supervoxel methods is the modeling of the relationship between spatial and temporal domains in a video. We plan to study these important questions in future work.

Acknowledgements This work was partially supported by the National Science Foundation CAREER grant (IIS-0845282), the Army Research Office (W911NF-11-1-0090) and the DARPA Mind's Eye program (W911NF-10-2-0062). We are grateful to the authors of the code and datasets that we have relied upon in this study, and we are grateful to the reviewers' comments, which have greatly improved this paper.

References

- Achanta R, Shaji A, Smith K, Lucchi A, Fua P, Susstrunk S (2012) Slic superpixels compared to state-of-the-art superpixel methods. *IEEE Transactions on Pattern Analysis and Machine Intelligence*
- Arbelaez P, Maire M, Fowlkes C, Malik J (2011) Contour detection and hierarchical image segmentation. *IEEE Transactions on Pattern Analysis and Machine Intelligence* 33(5):898–916
- Baker S, Scharstein D, Lewis J, Roth S, Black MJ, Szeliski R (2011) A database and evaluation methodology for optical flow. *International Journal of Computer Vision* 92(1):1–31
- Van den Bergh M, Roig G, Boix X, Manen S, Van Gool L (2013) Online video seeds for temporal window objectness. In: *IEEE International Conference on Computer Vision*
- Brendel W, Todorovic S (2009) Video object segmentation by tracking regions. In: *IEEE International Conference on Computer Vision*
- Brostow GJ, Shotton J, Fauqueur J, Cipolla R (2008) Segmentation and recognition using structure from motion point clouds. In: *European Conference on Computer Vision*
- Budvytis I, Badrinarayanan V, Cipolla R (2011) Semi-supervised video segmentation using tree structured graphical models. In: *IEEE Conference on Computer Vision and Pattern Recognition*
- Chang J, Wei D, III JWF (2013) A video representation using temporal superpixels. In: *IEEE Conference on Computer Vision and Pattern Recognition*
- Chen AYC, Corso JJ (2010) Propagating multi-class pixel labels throughout video frames. In: *Proceedings of Western New York Image Processing Workshop*
- Comaniciu D, Meer P (2002) Mean shift: A robust approach toward feature space analysis. *IEEE Transactions on Pattern Analysis and Machine Intelligence* 24(5):603–619
- Corso JJ, Sharon E, Dube S, El-Saden S, Sinha U, Yuille A (2008) Efficient multilevel brain tumor segmentation with integrated bayesian model classification. *Medical Imaging, IEEE Transactions on* 27(5):629–640
- DeMenthon D, Megret R (2002) Spatio-temporal segmentation of video by hierarchical mean shift analysis. In: *Statistical Methods in Video Processing Workshop*
- Drucker F, MacCormick J (2009) Fast superpixels for video analysis. In: *IEEE Workshop on Motion and Video Computing*
- Erdem ÇE, Sankur B, Tekalp AM (2004) Performance measures for video object segmentation and tracking. *IEEE Transactions on Image Processing* 13(7):937–951
- Felzenszwalb PF, Huttenlocher DP (2004) Efficient graph-based image segmentation. *International Journal of Computer Vision* 59(2):167–181
- Fowlkes C, Belongie S, Malik J (2001) Efficient spatiotemporal grouping using the nystrom method. In: *IEEE Conference on Computer Vision and Pattern Recognition*
- Fowlkes C, Belongie S, Chung F, Malik J (2004) Spectral grouping using the nyström method. *IEEE Transactions on Pattern Analysis and Machine Intelligence* 26(2):214–225
- Fukunaga K, Hostetler L (1975) The estimation of the gradient of a density function, with applications in pattern recognition. *IEEE Transactions on Information Theory* 21(1):32–40
- Galasso F, Cipolla R, Schiele B (2012) Video segmentation with superpixels. In: *Asian Conference on Computer Vision*
- Galasso F, Nagaraja NS, Cardenas TJ, Brox T, Schiele B (2013) A unified video segmentation benchmark: Annotation, metrics and analysis. In: *IEEE International Conference on Computer Vision*
- Gould S, Fulton R, Koller D (2009) Decomposing a scene into geometric and semantically consistent regions. In: *IEEE International Conference on Computer Vision*
- Greenspan H, Goldberger J, Mayer A (2004) Probabilistic space-time video modeling via piecewise gmm. *IEEE Transactions on Pattern Analysis and Machine Intelligence* 26(3):384–396
- Grundmann M, Kwatra V, Han M, Essa I (2010) Efficient hierarchical graph-based video segmentation. In: *IEEE Conference on Computer Vision and Pattern Recognition*
- Hanbury A (2008) How do superpixels affect image segmentation? In: *Progress in Pattern Recognition, Image Analysis and Applications*, Springer, pp 178–186
- He X, Zemel RS, Ray D (2006) Learning and incorporating top-down cues in image segmentation. In: *European Conference on Computer Vision*
- Hoiem D, Efros AA, Hebert M (2005) Automatic photo pop-up. In: *ACM Transactions on Graphics, ACM*, vol 24, pp 577–584

- Khan S, Shah M (2001) Object based segmentation of video using color, motion and spatial information. In: IEEE Conference on Computer Vision and Pattern Recognition
- Kläser A, Marszałek M, Schmid C (2008) A spatio-temporal descriptor based on 3d-gradients. In: British Machine Vision Conference
- Laptev I (2005) On space-time interest points. *International Journal of Computer Vision* 64(2):107–123
- Lee J, Choi S (2014) Incremental tree-based inference with dependent normalized random measures. In: Proceedings of the Seventeenth International Conference on Artificial Intelligence and Statistics, pp 558–566
- Lee YJ, Kim J, Grauman K (2011) Key-segments for video object segmentation. In: IEEE International Conference on Computer Vision
- Levinshstein A, Stere A, Kutulakos KN, Fleet DJ, Dickinson SJ, Siddiqi K (2009) Turbopixels: Fast superpixels using geometric flows. *IEEE Transactions on Pattern Analysis and Machine Intelligence* 31(12):2290–2297
- Li F, Kim T, Humayun A, Tsai D, Rehg JM (2013) Video segmentation by tracking many figure-ground segments. In: IEEE International Conference on Computer Vision
- Liu C, Freeman WT, Adelson EH, Weiss Y (2008a) Human-assisted motion annotation. In: IEEE Conference on Computer Vision and Pattern Recognition
- Liu MY, Tuzel O, Ramalingam S, Chellappa R (2011) Entropy rate superpixel segmentation. In: IEEE Conference on Computer Vision and Pattern Recognition
- Liu S, Dong G, Yan CH, Ong SH (2008b) Video segmentation: Propagation, validation and aggregation of a preceding graph. In: IEEE Conference on Computer Vision and Pattern Recognition
- Megret R, DeMenthon D (2002) A survey of spatio-temporal grouping techniques. Tech. rep., UMD
- Moore AP, Prince S, Warrell J, Mohammed U, Jones G (2008) Superpixel lattices. In: IEEE Conference on Computer Vision and Pattern Recognition
- Mori G, Ren X, Efros AA, Malik J (2004) Recovering human body configurations: Combining segmentation and recognition. In: IEEE Conference on Computer Vision and Pattern Recognition
- Palou G, Salembier P (2013) Hierarchical video representation with trajectory binary partition tree. In: IEEE Conference on Computer Vision and Pattern Recognition
- Paris S (2008) Edge-preserving smoothing and mean-shift segmentation of video streams. In: European Conference on Computer Vision
- Paris S, Durand F (2007) A topological approach to hierarchical segmentation using mean shift. In: IEEE Conference on Computer Vision and Pattern Recognition
- Patel NV, Sethi IK (1997) Video shot detection and characterization for video databases. *Pattern Recognition* 30(4):583–592
- Ren X, Malik J (2003) Learning a classification model for segmentation. In: IEEE International Conference on Computer Vision
- Reso M, Jachalsky J, Rosenhahn B, Ostermann J (2013) Temporally consistent superpixels. In: IEEE International Conference on Computer Vision
- Schmid C, Mohr R (1997) Local grayvalue invariants for image retrieval. *IEEE Transactions on Pattern Analysis and Machine Intelligence* 19(5):530–535
- Sharon E, Brandt A, Basri R (2000) Fast multiscale image segmentation. In: IEEE Conference on Computer Vision and Pattern Recognition
- Sharon E, Galun M, Sharon D, Basri R, Brandt A (2006) Hierarchy and adaptivity in segmenting visual scenes. *Nature* 442(7104):810–813
- Shi J, Malik J (2000) Normalized cuts and image segmentation. *IEEE Transactions on Pattern Analysis and Machine Intelligence* 22(8):888–905
- Shotton J, Winn J, Rother C, Criminisi A (2009) Textonboost for image understanding: Multi-class object recognition and segmentation by jointly modeling texture, layout, and context. *International Journal of Computer Vision* 81(1):2–23
- de Souza KJF, de Albuquerque Araújo A, et al (2014) Graph-based hierarchical video segmentation based on a simple dissimilarity measure. *Pattern Recognition Letters*
- Sundberg P, Brox T, Maire M, Arbeláez P, Malik J (2011) Occlusion boundary detection and figure/ground assignment from optical flow. In: IEEE Conference on Computer Vision and Pattern Recognition
- Tighe J, Lazebnik S (2010) Superparsing: scalable nonparametric image parsing with superpixels. *International Journal of Computer Vision*
- Tripathi S, Hwang Y, Belongie S, Nguyen T (2014) Improving streaming video segmentation with early and mid-level visual processing. In: IEEE Winter Conference on Applications of Computer Vision
- Tsai D, Flagg M, Rehg JM (2010) Motion coherent tracking with multi-label mrf optimization. In: British Machine Vision Conference
- Vazquez-Reina A, Avidan S, Pfister H, Miller E (2010) Multiple hypothesis video segmentation from superpixel flows. In: European Conference on Computer Vision
- Veksler O, Boykov Y, Mehrani P (2010) Superpixels and supervoxels in an energy optimization framework. In: European Conference on Computer Vision
- Vincent L, Soille P (1991) Watersheds in digital spaces: an efficient algorithm based on immersion simulations. *IEEE Transactions on Pattern Analysis and Machine Intelligence* 13(6):583–598
- Wang H, Kläser A, Schmid C, Liu CL (2013) Dense trajectories and motion boundary descriptors for action recognition. *International Journal of Computer Vision*

- Wang J, Thiesson B, Xu Y, Cohen M (2004) Image and video segmentation by anisotropic kernel mean shift. In: European Conference on Computer Vision
- Xu C, Corso JJ (2012) Evaluation of super-voxel methods for early video processing. In: IEEE Conference on Computer Vision and Pattern Recognition
- Xu C, Xiong C, Corso JJ (2012) Streaming hierarchical video segmentation. In: European Conference on Computer Vision
- Xu C, Whitt S, Corso JJ (2013) Flattening supervoxel hierarchies by the uniform entropy slice. In: IEEE International Conference on Computer Vision
- Zeng G, Wang P, Wang J, Gan R, Zha H (2011) Structure-sensitive superpixels via geodesic distance. In: IEEE International Conference on Computer Vision